City Research Online

City St George's, University of London

Citation: Lockett, R. D. (2006). Instabilities and soot formation in spherically expanding, high pressure, rich, iso-octane-air flames. Journal of Physics: Conference Series, 45, pp. 154-160. doi: 10.1088/1742-6596/45/1/020

This is the unspecified version of the paper.

This version of the publication may differ from the final published version. To cite this item please consult the publisher's version.

Permanent repository link: https://openaccess.city.ac.uk/id/eprint/2141/

Link to published version: https://doi.org/10.1088/1742-6596/45/1/020

Copyright and Reuse: Copyright and Moral Rights remain with the author(s) and/or copyright holders. Copies of full items can be used for personal research or study, educational, or not-for-profit purposes without prior permission or charge, unless otherwise indicated, provided that the authors, title and full bibliographic details are credited, a hyperlink and/or URL is given for the original metadata page and the content is not changed in any way. For full details of reuse please refer to City Research Online policy.

City Research Online: http://openaccess.city.ac.uk/ publications@citystgeorges.ac.uk

Institute of Physics Publishing Journal of Physics: Conference Series **45** (2006) 154–160
doi:10.1088/1742-6596/45/1/020 Second International Conference on Optical and Laser Diagnostics (ICOLAD 2005)

Instabilities and soot formation in spherically expanding, high pressure, rich, iso-octane-air flames

R D Lockett

School of Engineering and Mathematical Sciences, City University, Northampton Square, London EC1V OHB

russel.lockett@ntlworld.com

Abstract: Flame instabilities, cellular structures and soot formed in high pressure, rich, spherically expanding iso-octane-air flames have been studied experimentally using high speed Schlieren cinematography, OH fluorescence, Mie scattering and laser induced incandescence. Cellular structures with two wavelength ranges developed on the flame surface. The larger wavelength cellular structure was produced by the Landau-Darrieus hydrodynamic instability, while the short wavelength cellular structure was produced by the thermal-diffusive instability. Large negative curvature in the short wavelength cusps caused local flame quenching and fracture of the flame surface. In rich flames with equivalence ratio $\phi > 1.8$, soot was formed in a honeycomb-like structure behind flame cracks associated with the large wavelength cellular structure induced by the hydrodynamic instability. The formation of soot precursors through low temperature pyrolysis was suggested as a suitable mechanism for the initiation of soot formation behind the large wavelength flame cracks..

1. Introduction

If a deformation occurs in the surface of a spherically expanding laminar flame during its early development, any potential instabilities (hydrodynamic, thermal-diffusive) will be stabilised by the flame stretch until a critical Peclet number is reached. After this critical point, the flame may become unstable to surface perturbations, which can grow on the flame surface through the development of propagating cracks or cellular fission [1].

If the Lewis number for the deficient reactant in the fuel-air mixture is below a critical value, then in general, a perturbation in the expanding flame front is unstable. The perturbation grows as a consequence of an increase in enthalpy and local burning velocity along the crest of the perturbation, with a corresponding decrease in enthalpy and local burning velocity along the trough of the perturbation. However, if the Lewis number for the deficient reactant in the fuel-air mixture is above a critical value, then the flame front is stable to perturbations on the surface. Generally, this means that for fuel-air mixtures where the molecular mass of the fuel is considerably smaller than the molecular mass of air, lean flames are unstable to surface perturbations. The converse is also true for rich flames. This kind of flame instability is known as a thermal-diffusive instability. There are some exceptions to this general rule. Rich ethylene- and ethane-air flames have been observed to develop thermal-diffusive cracking [2].

© 2006 IOP Publishing Ltd

The second type of flame instability examined here is hydrodynamic in origin. Flame surface perturbations cause local pressure and density variations ahead of the advancing flame front, which can accelerate surface cracking. Hydrodynamic instabilities can be distinguished from thermal-diffusive instabilities through the identification of the different wavelengths associated with the two mechanisms. Furthermore, pressure oscillations ahead of the advancing flame front identify the presence of hydrodynamic instabilities. In practice, initial perturbations in a spherically expanding flame surface occur as a consequence of the mode of ignition, whether by a spark plug, or laser, or other means.

Fully developed flame cellularity due to thermal-diffusive cracking is distinguished from hydrodynamic cracking in that flames that hydrodynamically crack do not develop a discrete cellular structure as described above, unless of course the flame is unstable to thermal-diffusive cracking as well.

2. Experimental

Cracking in spherically expanding laminar flames was investigated using Shlieren cinematography [3], and hydroxyl Planar Laser Induced Fluorescence (PLIF) [4]. The flames were generated in the fan stirred bomb at Leeds University. The bomb is a spherical vessel of volume 31 litres, with six 190mm diameter optically accessible windows, and four tetrahedrally oriented fans. The vessel was designed to allow explosions of hydrocarbon-air mixtures to be undertaken at pressures of up to 15 bar [5].

Soot formed during explosions of rich iso-octane-air mixtures at high pressure was investigated using laser induced incandescence (LII) and Mie scattering in the optically accessible bomb at Shell, Thornton. Details of the experiments can be obtained from Tait [6] and Lockett et al [7, 8].

Schlieren cinematography was employed to investigate the evolution of the long wavelength cellular structure on the surface of the expanding flames, induced by the hydrodynamic instability. OH PLIF was employed to investigate the instantaneous structure of the unstable flames at a fixed radius (Peclet number) as a function of equivalence ratio and unburned mixture pressure. Simultaneous LII and Mie scattering was employed to identify any special characteristics of the soot formed in high pressure, rich, iso-octane-air flames.

The OH PLIF measurements were conducted in the Leeds bomb using a Lambda Physik EMG 150 MSC excimer laser, operating in narrow band tunable mode at 308.24nm. Laser light at this wavelength excites the $Q_1(3)$ line in the 0 - 0 band of the $A \leftarrow X$ transition in OH. The EMG 150 laser produced pulses of approximately 20ns duration, and 135mJ energy. The laser light was directed through a 2m spherical lens and a cylindrical telescope, producing a laser sheet of 67mm height, and 0.2mm width in the centre of the bomb. The fluorescence from the excited OH was on-resonance, and was imaged onto a lens coupled intesified CCD camera. The experimental configuration is shown schematically in Figure 1 below.

The flames were initiated from the centre of the bomb using single kernel spark plug ignition. Cracking in spherically expanding laminar flames was investigated for stoichiometric methane-air flames at 5 bar and 10 bar pressure, stoichiometric iso-octane-air flames at 5 bar and 10 bar pressure, equivalence ratio $\phi = 1.4$ iso-octane-air flames for pressures of one to five bar, at one bar intervals, and nitrogen diluted lean hydrogen-oxygen flames at one bar pressure. The nitrogen/hydrogen/oxygen mixture ratio was $N_2:H_2:O_2::10:3:2$.

The Shell high pressure bomb had a combustion chamber 8 cm in diameter, with four 30mm windows at right angles to each other in a plane across the centre of the bomb. The base of the bomb had a large viewing window for imaging purposes. The flame was ignited from the bottom corner of the

bomb using a conventional spark ignition unit, and the resulting flame kernel propagated towards the measurement zone where the soot LII/Mie scattering was produced.

LII/Mie scattering measurements in the Shell high pressure bomb were conducted using a Spectra Physics GCR-270 laser operating at 532nm. The laser produced single longitudinal mode (s.l.m.) pulses of 7ns to 9ns duration, and 500 mJ per pulse. The 532nm laser light was formed into a 2-d sheet using a 1m spherical lens, a -25mm diverging cylindrical lens and a +150mm converging cylindrical lens. The converging cylindrical lens was placed such that the laser sheet gently converged to a 30mm wide sheet at the entrance window to the bomb. The edges of the sheet were also masked by the 50mm diameter converging cylindrical lens.

The LII and Mie scattering from soot structures generated in the flame was imaged through the window in the base of the bomb. The LII and Mie scattering were separated into different optical paths, and then directed onto two separate ICCD cameras.

3. Results

Figure 1 shows a Schlieren image of a stoichiometric iso-octane-air spherical explosion flame obtained in the Leeds bomb at 5 bar pressure [3]. The flame radius is approximately 60 mm (Peclet no. ≈ 600). Surface wrinkling with a lengthscale of approximately 5 mm to 1 cm is observable, with a smooth surface between the wrinkle lines.

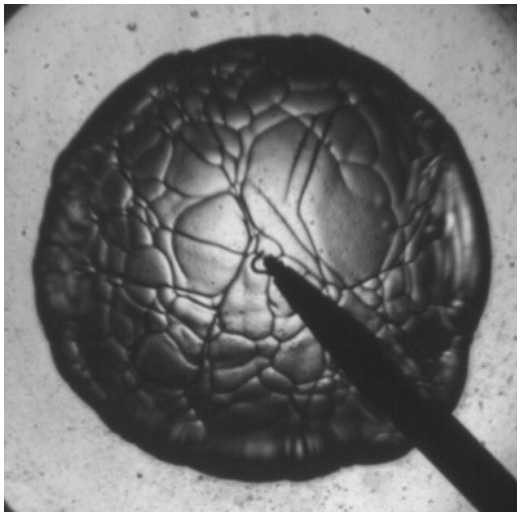

Figure 1: Schlieren Image of a 5 bar Stoichiometric Iso-octane-Air Explosion Flame obtained in the Leeds Bomb (Flame radius ≈ 60 mm)

Figure 2 below shows an unprocessed OH PLIF image of a stoichiometric iso-octane-air flame at 5 bar, obtained in the Leeds bomb [4]. The image width is 55mm, and the flame radius is approximately 60 mm. The flame is propagating downward in the image. Note that the length scales associated with the cracks in the flame front in the image corresponds to the wrinkling length scale observed in Figure 1 above. These cracks are formed as a result of the hydrodynamic instability, as the flame is stable to the thermal-diffusive instability.

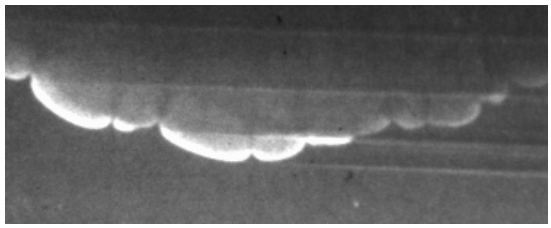

Figure 2: Unprocessed OH PLIF Image of a 5 bar Stoichiometric Iso-octane-Air Explosion Flame obtained in the Leeds Bomb (Flame radius ≈ 60 mm)

Figure 3 below shows a Schlieren image of a $\varphi = 1.4$ iso-octane-air spherical explosion flame obtained in the Leeds bomb at 5 bar pressure [3]. The flame diameter is approximately 60 mm (Peclet no. ≈ 600). Surface wrinkling with a lengthscale range of approximately 5 mm to 1 cm is observable as before. In addition, there is a fine structure superimposed on the larger surface wrinkles.

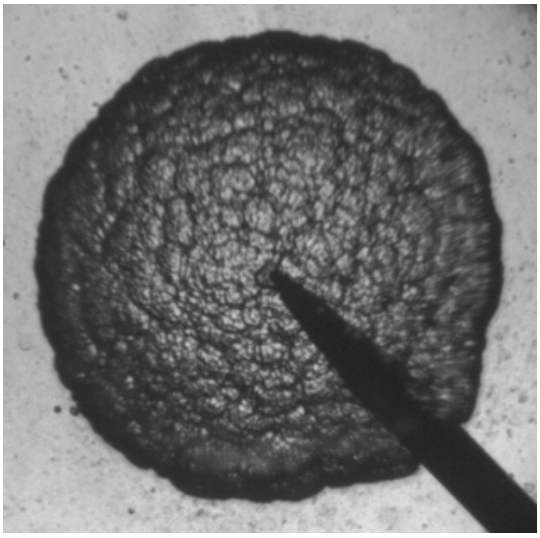

Figure 3: Schlieren Image of a 5 bar, $\varphi = 1.4$ Iso-octane-Air Explosion Flame obtained in the Leeds Bomb (Flame radius ≈ 60 mm)

Figure 4 below shows an unprocessed OH PLIF image of an equivalence ratio $\phi = 1.4$ iso-octane-air flame at 5 bar, obtained from the Leeds bomb [4]. As with the image in Figure 2 above, the flame is propagating downward. The image in the unburnt region of the flame is Rayleigh scattering from iso-octane and air at 5 bar. The flame surface has a cellular structure, with two discrete ranges of length scale exhibited. The flame cracks with the larger length scale range are determined by the hydrodynamic instability, and the smaller length scale cells are determined by the thermal-diffusive instability. The larger hydrodynamic instability length scale is comparable with the cracking length scale observed in Figure 1 and Figure 2 above.

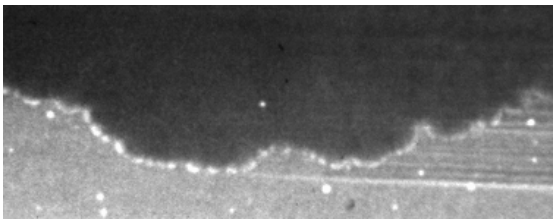

Figure 4: Unprocessed OH PLIF Image of a 5 bar, φ = 1.4 Iso-octane-Air Explosion Flame obtained in the Leeds Bomb (Flame radius ≈ 60 mm)

Figure 5 below shows a processed OH PLIF image of the nitrogen diluted hydrogen-oxygen explosion flame (1 bar pressure). The grey scale bar shows the OH molar density in the flame zone in units of mole/m^3. The OH concentration between the cells drops to near equilibrium values, indicating oxidation quenching in these zones. Flame quenching in the cusps is a consequence of the large negative curvature.

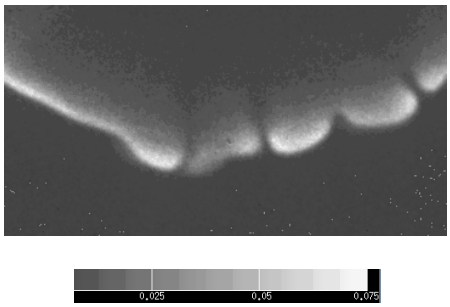

Figure 5: Processed OH PLIF Image of a 1 bar Lean Hydrogen-Oxygen Explosion Flame in an Enriched Nitrogen Atmosphere (OH Molar Concentration (mole/m^3))

Figure 6 shows a graph of the OH molar density through the flame as a function of flame radius.

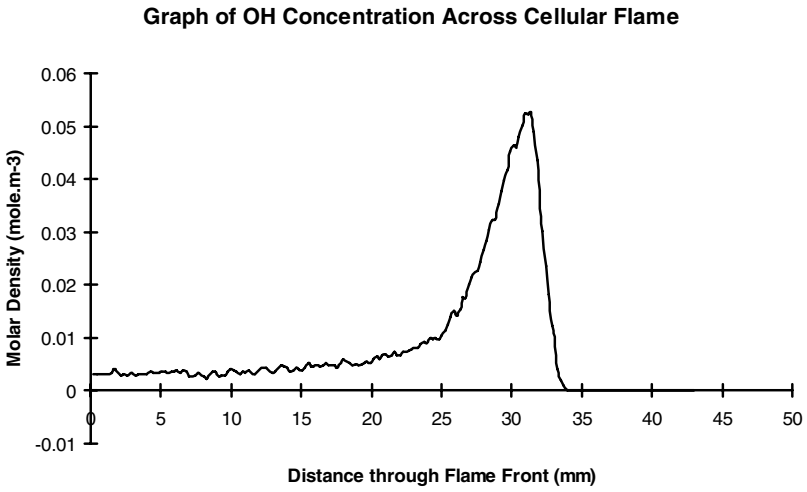

Figure 6: OH Concentration as a Function of Flame Radius

Figure 7 shows processed LII images obtained from soot formed behind φ = 1.8 iso-octane-air explosion flames obtained from the Shell bomb with an initial pressure of 5 bar [7]. The soot formed behind the flame forms a honeycomb-like structure, reflecting the history of the dynamic evolution of the flame surface. The LII images reflect relative soot volume fraction.

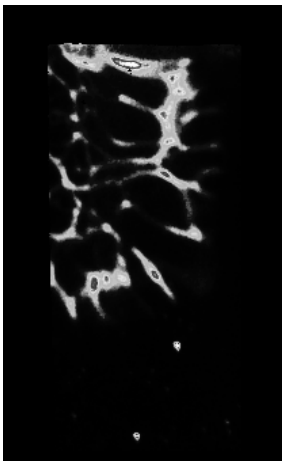

Figure 7: Relative Soot Volume Fraction from a φ = 1.8 Iso-octane-Air Explosion Flame obtained in the Shell Bomb (Initial pressure = 5 bar, Flame radius ≈ 60mm)

The processed LII image shown in Figure 7 is similar to the image data produced by Tait [6]. These images reveal that soot is formed behind deep cracks in the flame front. A characteristic length scale defining the soot cell size is observed to be of the order of 5 mm to 1 cm in length. This corresponds with the larger cellular length scale observed in Figures 3 and 4 above, determined by the hydrodynamic instability.

The formation of soot behind deep cracks on the flame surface suggests a simple mechanism. An element of unburned mixture following a flowline into a deep cusp in the flame surface experiences significant oxygen diffusion towards the local flame front. This depletes the fluid element of oxygen, enriching the local unburned mixture. This locally enriched mixture can exceed the rich flammability limit, causing local flame quenching in the cusp. The enriched fluid element enters the quenched cusp, slowly heats through molecular and heat diffusion obtained from the burned gas products, until the fuel reaches pyrolysis temperature. The fuel pyrolyses to form a range of molecules, including PAH molecules and other soot precursors. These molecules then combine to form soot. This is why the cellular soot structure reflects the history of the large scale cellular evolution of the flame.

4. Conclusion

1. Two distinct length scales associated with flame cracking have been observed from the Schlieren images and the OH PLIF images.

2. These length scales are identified with hydrodynamic effects and thermal-diffusive effects. The large length scale cracking (5 mm to 1 cm) is associated with the hydrodynamic instability, while the small length scale cracking is associated with the thermal-diffusive instability (~ 1 mm).

3. High pressure flames that are stable to thermal-diffusive cracking develop hydrodynamic cracks which do not develop into discrete cells, while high pressure flames unstable to thermal-diffusive cracking exhibit full cellular structure and hydrodynamic perturbations.

4. Flame reaction quenching has been observed in the regions between the smaller length scale flame cells.

5. In highly enriched, high pressure explosion flames ($\varphi > 1.8$), soot was observed to be formed in a honeycomb-like structure behind the flame.

6. The soot cell size was observed to be of the order of 5 mm to 1 cm, which corresponded with the larger length scale cellularity, determined by the hydrodynamic instability.

7. A plausible hypothesis for the formation of soot in highly enriched, spherical explosion flames was suggested.

References

1. D. Bradley, C.M. Harper; "The development of instabilities in laminar explosion flames", Twenty-Fifth Symposium (International) on Combustion, The Combustion Institute 1994.
2. G. Patnaik, K. Kailasanath, E.S. Oran, K. Laskey, "Detailed Numerical Simulations of Cellular Flames", Twenty-Second Symposium (International) on Combustion, p1517, The Combustion Institute 1989.
3. A. S. Al-Shahrany, D. Bradley, M. Lawes and R. Woolley, “Measurement of Unstable Burning Velocities of Iso-octane-air Mixtures at High Pressure and the Derivation of Laminar Burning Velocities”, Thirtieth Symposium (International) on Combustion, The Combustion Institute 2004.
4. D. Bradley, C.G.W. Sheppard, R. Woolley, D.A. Greenhalgh, R.D. Lockett, “The Development and Structure of Flame Instabilities and Cellularity at Low Markstein Numbers in Explosions”, Combustion and Flame 122: pp 195 – 209, 2000
5. D. Bradley, M. Lawes, C.G.W. Sheppard, R. Woolley, "Turbulent Flame Speeds", Contract: JOU2-CT92-0081: Final Report 1.7.93 to 51.5.95
6. N.P. Tait, Combustion and Flame 117: pp 435 – 438, 1999
7. R.D. Lockett, V. Grigorian, D.A. Greenhalgh, Optical Diagnostics in Applied Combustion (EU-ZODIAC), Soot Package Final Report, December 1997
8. R.D. Lockett, N.P. Tait, D.A. Greenalgh, to be published, 2006